High Velocity Flows Inside Tube Reactors

Shahana Chatterjee[1,2*], Thomas Abadie[3,4], Meihui Wang[1], Omar K. Matar[3], Rodney S. Ruoff[1,5,6,7*]

1. *IBS Center for Multidimensional Carbon Materials, Ulsan 44919, Republic of Korea*
2. *Make Materials, Toronto, Canada*
3. *Department of Chemical Engineering, Imperial College London, London SW7 2AZ, United Kingdom*
4. *School of Chemical Engineering, University of Birmingham, Birmingham B15 2TT, United Kingdom*
5. *Department of Chemistry, Ulsan National Institute of Science and Technology (UNIST), Ulsan 44919, Republic of Korea*
6. *Department of Materials Science, UNIST, Ulsan 44919, Republic of Korea*
7. *School of Energy and Chemical Engineering, UNIST, Ulsan 44919, Republic of Korea*

chatterjee.shahana@gmail.com, ruofflab@gmail.com, rsruoff@ibs.re.kr

Abstract

Tube reactors used for the chemical vapor deposition of graphene and other 2D films on metal foils are typically operated at ambient pressures or under low vacuum (> 0.1 torr) and at low average flow velocities (< ~1-2 m/s) and Reynolds numbers (< 100). Thus, the flow inside the reactor is laminar and highly diffusive. This report explores what may happen if high velocity flows are instead used, by simulating reactor conditions with the Computational Fluid Dynamics toolbox OpenFOAM. High velocity flows with large Reynolds numbers were found to be turbulent and without any buoyancy driven recirculation. Additionally, a large cooling effect was observed with foil and gas temperatures much lower than the furnace set point. Finally, the temperatures of the 50-100 μm thick metal foils were not uniform but had large temperature gradients sensitive to the system pressure, the total mass flow rate and the process gas composition that increased with decreasing foil thickness.

Keywords: Computational Fluid Dynamics (CFD), OpenFOAM, heat transfer, tube reactor

Introduction

Typical hot-wall tube reactors (heated by an external furnace) are operated under low (> 0.1 torr) or ambient pressures and low flow velocities and Reynolds numbers (*Re*), for the chemical vapor deposition (CVD) of graphene and other 2D films on metal foils. Under such conditions, it was observed that the flows were mostly diffusive with thick (momentum and concentration) boundary layers (BLs) and that the metal foils and the surrounding fluid were heated uniformly in the hot-zone of the reactor (with temperatures close to the furnace set-point). Moreover, the flows were often characterized by large Rayleigh (*Ra*) and Richardson (*Ri*) numbers with significant buoyancy driven recirculation observed upstream and downstream to the heated metal foils.[1] In this paper, we have explored what happens when the average flow velocities are much higher, but at similar system pressures and temperatures. Such flows are characterized by larger *Re* and *Ra* but lower *Ri*, and are thus expected to be much less diffusive with minimal or no buoyancy driven recirculation (buoyancy driven recirculation was observed only when both *Ra* and *Ri* were high).

Results and Discussion

Reactor and Process Details

The reactor tube had an inner diameter of 0.046 m and was 1.5 m long (**Figure ST-0**). The reactor inlet had an inner diameter of 0.004 m (**Table ST-2**). The metal foil (of copper) was 100 μm thick unless otherwise mentioned. This 2 cm long and 4 cm wide foil was positioned at a distance of 0.6 m (**foil setup A**, default setup) or of 0.75 m (**foil setup B**) from the inlet. A thermal profile ~1.2 m long and with a maximum temperature of 1293 K was applied to the wall of the reactor tube (**Figure ST-0**). Different system pressures at the reactor outlet and different process gas compositions have been considered.

Methodology Selection

The Knudsen numbers for the process gases Ar, H_2 and CH_4 (a typical graphene precursor) at room temperature (RT, 293 K) and 1293 K are much less than 0.01. Hence, continuum mechanics was used. The reactor inlet was ~100 times smaller in area than the reactor, and a huge change in flow velocity and density were observed in the entrance region (**Table S1**). Moreover, heating the gases to very high temperatures also introduced large density variations in the flow. Thus, compressible solvers in OpenFOAM[2–4] were used to simulate the flow. As the reactor contained both fluid and solid regions, conjugate heat transfer inside the reactor was simulated by solving the energy equation for both the solid and the fluid phases and the continuity and the momentum equations for the fluid phase only. Again, radiation effects were also considered, as the reactor was heated to very high temperatures. Finally, after the flow properties were calculated, the transport of a passive scalar *s* (such as the graphene precursor CH_4) was studied by using a modified scalar transport equation.

Flow Dynamics in an Empty Tube Reactor at Room Temperature

Prior to simulating high temperature processes, the flow inside the empty reactor at RT was first explored (**condition T0**, **Table S2**). At 100 torr, an Ar only with an average inlet velocity of 146.61 ms^{-1} (**Table S2**) was studied. This flow had a *Re* of 5654 indicating a turbulent flow regime. Additionally, the greater than 100 times expansion in area from the inlet to the rest of the reactor tube introduced turbulence into the system. Thus, the flow inside the reactor was considered to be turbulent and solved with a turbulence model (the *k*-ω SST model, with details provided in the SI).

For the inlet velocity *U*, the empirical power-law velocity profile of a fully developed turbulent flow was adapted, with $n = 6$:

$$U(r) = U_c \left(1 - \frac{r}{R}\right)^{\frac{1}{n}}$$

where, U_c is the centerline or axial velocity, r is the radial distance from the centerline, and, R is the inlet radius.[5] The turbulent intensity Ti at the inlet was calculated based on the Re, as: $Ti = 0.16*Re^{-1/8}$; this was equivalent to a Ti of 5.4%. The turbulent kinetic energy per unit mass or k was calculated using this Ti and velocity profile as $k = 1.5*(T_i*U)^2$. The specific dissipation rate ω was set to a fixed value of 63614 s^{-1} based on the average velocity (please see SI for details). The outlet pressure of 100 torr was used as a fixed value boundary condition (BC). All solver details and BCs used can be found in **SI**.

The gas flowed into the reactor (**Figures 1**, **S1**) and expanded in a jet-like fashion with a significant drop in average velocity along the tube length, (for example, from ~180.5 ms^{-1} to ~2 ms^{-1} over a length of 13 cm along the tube axis). This velocity decrease introduced an adverse or positive pressure gradient in this region, and, it could be observed that the boundary layer (BL) had detached itself from the tube wall and a recirculation zone had developed. Right next to the inlet, this recirculation zone almost completely filled the tube, and, as the jet of gas expanded further down the tube, the spread of the recirculation zone across the tube decreased till the BL reattached itself to the tube walls. Again, in this region, large values of vorticity ξ, k, turbulent viscosity υ_t, specific dissipation rate ε and Ti were observed around the middle of the tube. The average Ti in the entrance region was ~18% i.e. a high turbulence intensity. All turbulence variables were found to gradually decrease farther downstream.

At the end of the recirculation zone, the BL reattached itself to the tube walls and started growing to fill the tube completely and towards a fully developed turbulent flow. The line profiles of k, ε and Ti across the tube diameters in **Figures 1**, **S1** showed expected trends: two symmetric peaks on the two sides of the centerline, while large ξ values (**Figure S1)** were now confined to the BL regions next to the tube walls. The $U_{magnitude}$ across the tube diameter had a turbulent

velocity profile that was mostly flat across the tube with a steep decrease to zero at the walls. The turbulence variables k, υ_t, ε and Ti continued to decrease further as turbulence in the flow gradually decreased and the flow transitioned from turbulent to laminar. On the other hand, a slow increase in $U_{magnitude}$ along the tube axis was observed as the reactor tube was not long enough for the flow to develop fully.

Flow Dynamics in a Tube Reactor with a Suspended Metal Foil at Room Temperature

In a separate simulation, the flow around a 100 μm copper foil when the reactor was at RT was studied (**foil setup A**, **condition T0**, **Table S2**). The flow was modified as expected when the foil was introduced into it and two new regions were formed: a new BL region around the foil and a wake region downstream to the foil (**Figure S2**). A stagnation line could be observed at the upstream edge of the foil, above and below which the fluid was deflected away from the foil. The BL region was also turbulent like the rest of the flow and increased in thickness (up to ~5-6 mm) from the upstream to the downstream edge of the foil. Thus, $U_{magnitude}$ showed stronger gradients normal to the foil at the upstream edge than at the downstream edge. The wake region was also turbulent, ~1 cm long, and, gradually merged with the rest of the flow. No adverse pressure gradients or any resultant BL separation or flow recirculation were observed, possibly because of the extreme thinness of the foil.

Flow Dynamics and Temperature Distribution of a Hot, Empty Tube Reactor

For simulating the heated empty tube (**condition T1**, **Table S2**), the furnace was centered at 0.6 m from the tube inlet, at -0.15 m; thus, the center of the 'hot-zone' of the reactor tube was also at this position. Ar gas has a Prandtl number (Pr) of 0.67. A turbulent Prandtl number (Pr_t) of 1.0 was used for this and all other heated tube simulations, in accordance to Reynolds analogy (also see SI). Thermal profile A started right from the inlet (at ~307 K) and continued for ~1.2 m

downstream. The fluid temperature also started increasing right after the inlet, and was greater than RT within the first 1 cm from the inlet. Similar to the tube at RT, a recirculation zone was also observed next to the inlet. There was almost no change in the values of the different flow variables in this part of the tube, possibly because the average temperature of the fluid, ~308 K showed only a small rise from RT. Further down the reactor, as the wall temperature increased further, the gas temperature increased, its density decreased and gas velocity increased. The wall temperature increased up to -0.15 m (i.e. up to the center of the hot zone) and then started decreasing; heat flow into the fluid could be observed with T_{wall} > gas $T_{average}$ till ~0 m (i.e. slightly downstream to the hot-zone center). Beyond ~0 m, gas $T_{average} > T_{wall}$ as a result of advection, and, the wall thus became a heat sink; near the outlet, T_{wall} ~293 K while gas $T_{average}$ ~463 K. All flow properties were dictated by this thermal field; regions of high *T* had lower densities and higher velocities (as mass flow rate i.e. $\rho*U*Area$ across the tube cross section must be conserved). Regions of higher *T* also had higher values of dynamic and kinematic viscosities; all these changes resulted in lower *Re* and decreased turbulence. For example, a 2 cm long region around the center of the hot-zone now had a *Ti* of ~2.15%, compared to ~6.19% when it was at RT. Similarly, all other turbulence variables were modified by this thermal field with lower values of *k* and υ_t at higher temperatures (**Figure S3**).

Flow Dynamics and Temperature Distribution of a Hot Reactor with a Suspended Metal Foil

Conjugate heat transfer simulations were then performed to calculate the temperature distribution across the 100 μm thick copper foil positioned at the center of the hot-zone (**foil setup A** and **condition T1**, **Table S2**). This was a multi-region simulation that calculated the temperature distribution across the foil. The edges of the foil touching the walls of the tube were at the same temperature as the tube-wall (this was provided as a fixed-value BC) while the central

part in-between was calculated to be at relatively lower temperatures (**Figure S4**, a parabolic profile could be observed along the foil width at a specific *z* value). Again, the upstream edge of the foil was found to be colder than the downstream edge (**Figure S4**, an exponential increase in temperature could be observed from the upstream to the downstream edge along the foil centerline). Thus, the foil had an overall temperature range of ~1202.51 – 1293 K, with an average temperature of ~1245.54 K. In contrast, temperatures were found to be uniform through the foil thickness and the top and the bottom surfaces had similar temperature distributions. Temperature gradients calculated for the foil showed higher gradients for lower temperature regions that experienced a greater cooling effect by the flow of gas.

With respect to the flow, the recirculation zone upstream to the foil remained identical to the previous simulations. The BL region of the hot foil could now be described in terms of both the momentum and the thermal BLs (**Figure S5**). In the thermal BL, the temperatures of the gas in contact with the foil were the same as the foil and gradually changed to the values of the surrounding gas. The thermal and momentum BLs had thicknesses that ranged up to ~6 mm and ~8 mm respectively (the *Pr* of 0.67 for Ar meant a thermal BL that was slightly thicker than the momentum BL). The thermal BL also increased in thickness from the upstream to the downstream edge of the foil, like the momentum BL and this was reflected in the higher temperature gradients at the upstream edge. Both the BL and wake regions were turbulent. The average gas temperature around the hot-zone center (i.e. around the foil) was only slightly higher (by ~10 K) than that of the heated empty tube (**Table S3**); hence, turbulence variables were also very similar. Hence, line profiles along the *x* and *y* diameters of the tube for k, υ_t, ε and *Ti* in the hot zone were more like those of the hot empty tube than those of the tube with foil at RT. Thus, it may be concluded that

introducing the copper foil to the heated tube produced only minor changes to its flow and thermal fields (**Table S3**).

The Contributions of Different Heating Modes on the Foil Temperature

The contributions of the different heating modes of the foil, namely, conduction, convection, and, radiation, were explored with the 100 μm Cu foil. Accordingly, different control experiments were simulated (**Table S4**) where a heating mode was artificially deactivated. It was observed that when the effects of radiation were not considered (**control H1**), foil temperatures barely decreased, owing to the low thermal emissivity of copper. When the foil edges no longer touched the hot tube wall but had a small gap of 2 mm (i.e. heat conduction from the tube wall to the foil was no longer possible, **control H2**), the foil average temperature decreased by ~267 K. When the foil touched the tube wall only partially, its temperature was still lower than the default case, but by much smaller amounts (**control H3**: ~27 K, **control H4**: ~23 K). Finally, when the gas velocity was reduced (i.e. minimal convection, by using a very small amount of gas at the same system pressure, **control H5**), the foil temperatures were nearly equal to the tube wall temperatures. (In all these cases, the average temperatures of the fluid around the foil at the center of the hot-zone were in a similar range, around ~738 – 739 K, while being slightly lower for **control H2** (~713 K) and much higher for **control T5** with a negligible gas flow (~1292 K)). Thus, the temperature of the copper foil was primarily driven by heat conduction (heating) and convection (cooling). Increased conduction was found to increase the foil temperature while a reduction in convection reduced cooling due to gas flow and hence also increased the foil temperature. This also implied that any changes in the flow conditions (gas velocity and system pressure) as well as foil position (whether and by how much it touches the tube wall) will possibly modify the temperature field of the foil.

The Effect of Process Gas Composition

Introducing H_2 into the system (1.23% H_2 by mass, 19.65% by moles, **condition A, Table S2**) produced fields that were similar to the ones with **condition T1** discussed above (**Figures S7, S8**). **Condition A** was also explored with a 50 μm foil (**Figures 2 , S6**) and the resultant fields were found to differ. Finally, the transport of the passive scalar *s*/ CH_4 was explored for both cases. The concentration BL in either case was similar to their respective momentum and thermal BLs with an increasing thickness and weaker gradients from the upstream to the downstream edge and followed by a small wake.

In order to understand the effect of H_2 gas on flow properties, two average inlet velocities (146.61 and 50.58 ms^{-1}) were studied, with different proportions of H_2 (with **foil setup A**, **Table S5**, **Figure 3** and **Figure S9**) in the Ar-H_2 mix. It was observed that at either velocity, with an increasing proportion of H_2, the fluid was hotter, with higher values of minimum and average temperatures around the foil in the hot-zone. In fact, for the H_2 only flow, the fluid temperatures in the hot-zone were found to be very close to the temperatures of the reactor wall. In comparison, foil temperatures were similar or higher (by smaller amounts than for the gas) than for the Ar only flow at the same mass flow rate. Again, the *Ti* in the fluid around the foil also decreased with higher amounts of H_2 in the mix, owing to its higher temperatures. Additionally, increased temperatures in the BL regions meant increased diffusion of the passive scalar *s* and thicker concentration BLs around the foil. The possible cause for increased temperatures with H_2 is its ~10 times higher thermal diffusivity compared to Ar.

The effect of changing both the average inlet velocity and the proportion of H_2 was then studied (with **foil setup A**, **Tables S6-S7**; **Figures 4**, **S10-S13**). Both foil and gas average

temperatures were found to decrease with increasing inlet average velocities and Ar mass fractions, along with thinner BLs.

Finally, H_2 only, He only, N_2 only and Ar only flows under the same conditions was compared. The flow fields were similar for Ar and N_2 while H_2 and He behaved similarly (**foil setup B**, **condition T1**, **Figure S14, Table S8**).

The Effect of Foil Thickness

As the calculated flow fields were found to differ between the 50 μm and the 100 μm foils under the same conditions, simulations were performed for a range of foil thicknesses (with **foil setup A** and **condition A**, **Table S9**, **Figure 5**). It was observed that as the foil thickness increased, both the minimum and the average foil temperatures increased. Moreover, the temperature distribution was much more uniform with smaller temperature gradients, for increasing foil thickness. Interestingly, even for a 1 mm thick foil, the top and the bottom surfaces had the same temperature distributions (**Figure S15**). In comparison, fluid temperatures remained almost the same. This trend was also observed for flow conditions other than **condition A** (**Table S9**). This increased sensitivity with decreasing thickness is possibly due to a decreasing thermal mass and a decreasing absolute area of contact between the foil and the hot tube wall while the same foil area was exposed to the flowing process gases. This implies reduced heating by conduction but similar amounts of cooling due to convection.

The Effects of Foil Holders

The foil may also be suspended with the help of a substrate holder, composed of a non-reactive material (like quartz, alumina or tungsten). Simulating the same process condition for these different setups can give different flow properties and foil temperatures (**Figures 6, S16**, **Table S10**). For example, when the foil is freely suspended with its edges touching the reactor

walls, its edges will have higher temperatures compared to the middle region, and its downstream side will be hotter than its upstream side. A similar distribution is observed for a foil placed horizontally on the top of a holder with its edges touching the holder. In comparison, when a foil is suspended vertically, its 'top' edge (from which it has been hung) is much hotter. Again, changing the material of the substrate holder from quartz to alumina or tungsten may result in different foil temperatures under the same reactor conditions because of their different thermal conductivities. However, the two surfaces of the foil were typically found to be at the same temperatures (**Figure S16**), possibly because of its thinness and high thermal conductivity.

Conclusion

We have found that (1) the tube reactor, operates under turbulent flow conditions. We have also found that (2) the copper foil temperature is not uniform and show an increasing sensitivity to the process gas composition, their average velocities and system pressure with decreasing thickness. Moreover, (3) the use of substrate holders may further modify the flow fields and foil temperatures.

Acknowledgements

This work was supported by IBS-R019-D1. S.C. and M.W. would like to thank Dr. Da Luo (IBS Center for Multidimensional Carbon Materials) and Dr. Won Kyung Seong (IBS Center for Multidimensional Carbon Materials) for help with measurements. S.C. would also like to thank late Prof. Meenakshi Chatterjee for discussions in 2008-2012 that inspired this work.

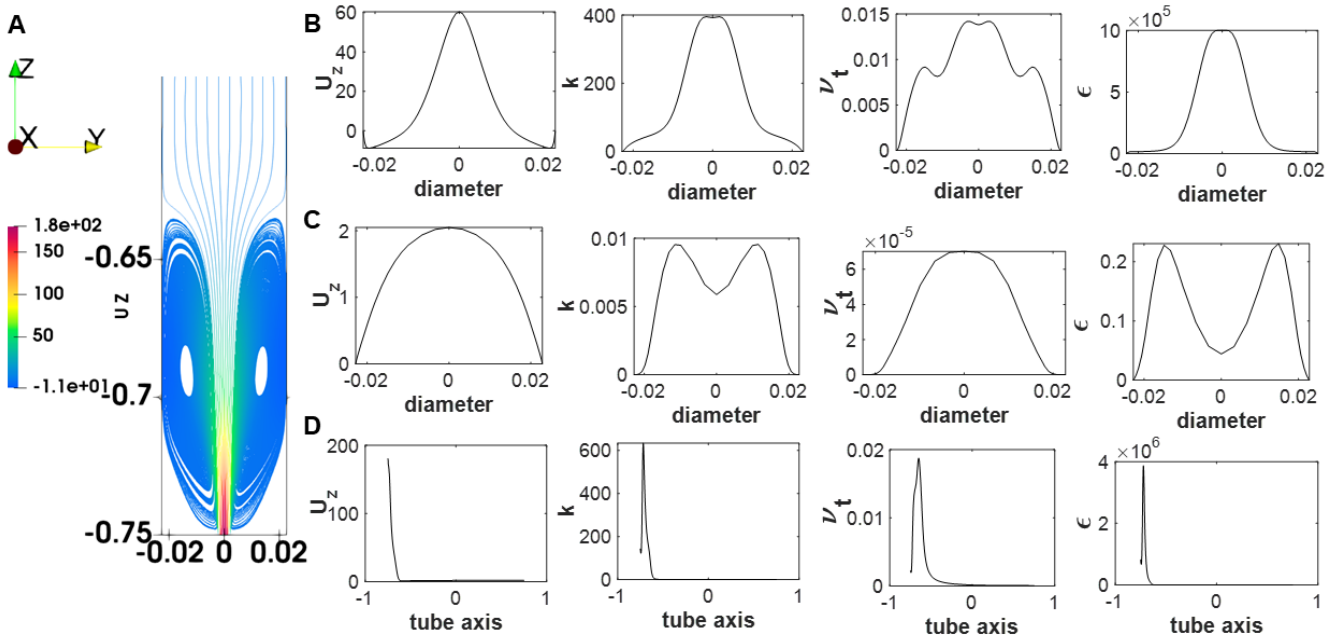

Figure 1. Flow inside an empty reactor tube with a Ar only flow at 100 torr and RT (**condition T0**): (A) *YZ* slice (axes in m, at x = 0 m) of the tube showing streamlines near the inlet (color coded with U_z); line profiles across the tube y diameter (m) at x = 0 m, and, (B) z = -0.7 m (entrance region), and, (C) z = 0.6 m; (D) along the tube axis (m). U_z is in ms^{-1}, k is in m^2s^{-2}, υ_t is in m^2s^{-1}, and, ε is in m^2s^{-3}.

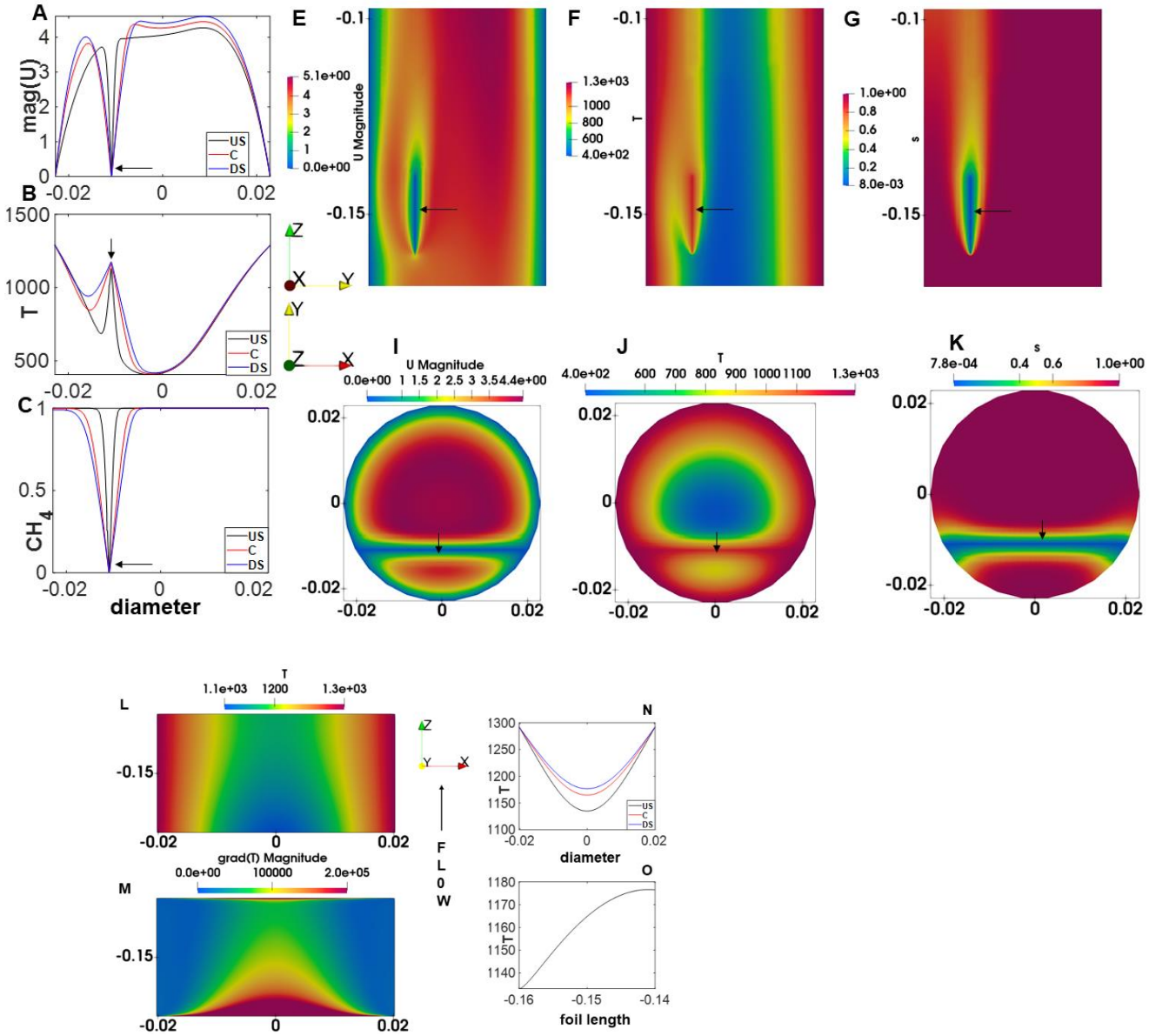

Figure 2. (A)-(C) Line profiles along the tube *y* diameter (m) at *x* = 0 m and across a 50 μm foil (with **setup A** and **condition A**) at *z* = -0.159 m (US, close to the foil upstream edge), at *z* = -0.15 m (C, at the foil center), and, at *z* = -0.141 m (DS, close to the foil downstream edge) for fields (A) mag(*U*) (ms^{-1}), (B) *T* (K), and, (C) normalized CH_4 concentration. (E)-(K): slices of the tube showing mag(*U*) (ms^{-1}) and *T* (K) fields of the process gases, and, normalized methane concentration (*s*) around the foil: (E)-(G) *YZ* slice (at *x* = 0 m), (I)-(K) *XY* slice (at *z* = -0.15 m) of the reactor tube, with all axes in m. (L) and (M) show the *T* (K) and grad(*T*) (Km^{-1}) on the foil surface (axes in m) respectively. (N) Line profiles across the width (m) of the foil (along *x*) at *z* = -0.159 m (US), *z* = = -0.15 m (C), and, *z* = -0.141 m (DS) through the middle of the foil (at *y* = -0.0109 m). (O) Line profile along the foil length (m) showing an exponential increase in *T* from upstream to downstream edge of foil (along *z*) through its middle (at *x* = 0 m, *y* = -0.0109 m). Arrows indicate foil location.

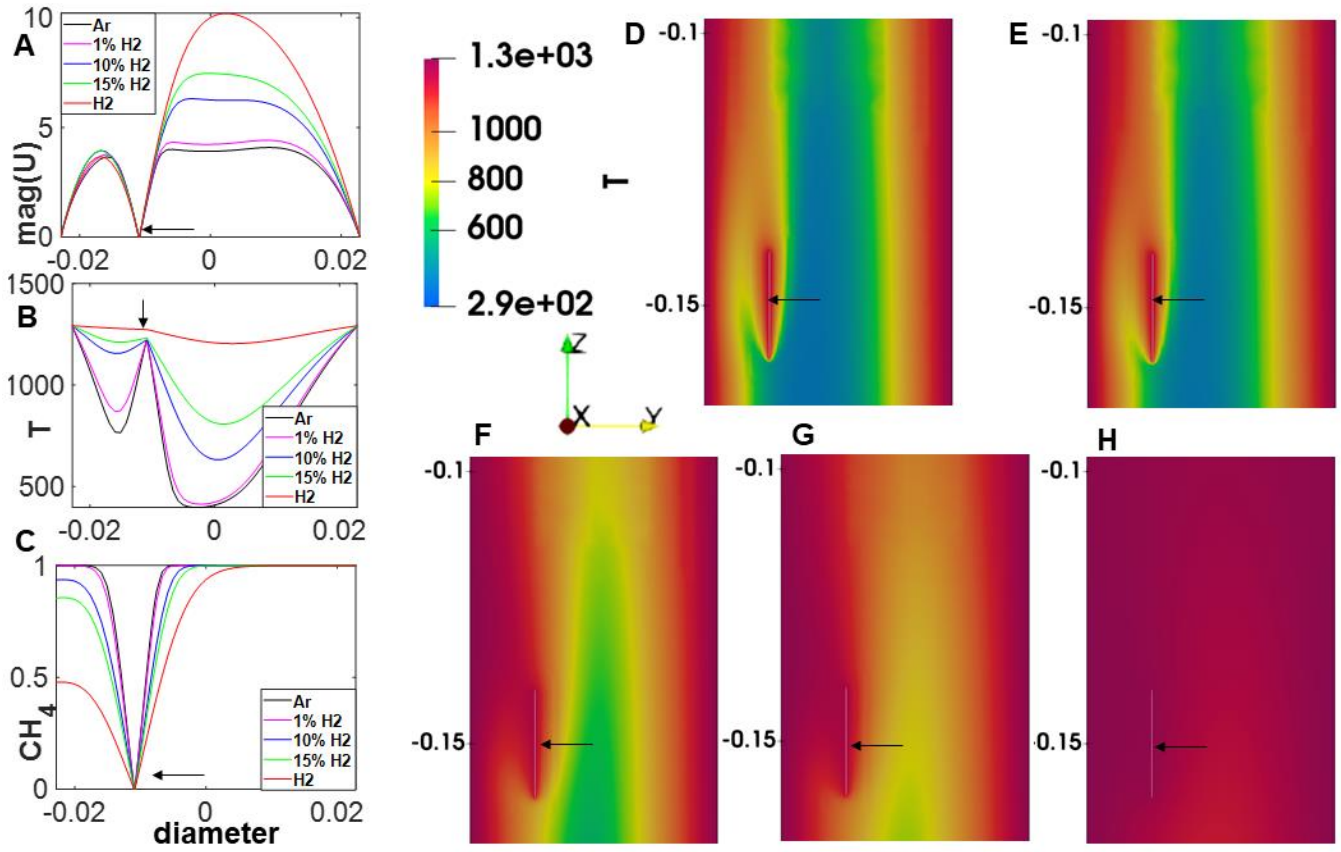

Figure 3. (A)-(C) Line profiles along the tube *y* diameter (m) at x = 0 m and across the center (at z = -0.15 m) of the 100 μm foil (with **foil setup A**) for flows with different mass% of H_2: (A) mag(U) (ms^{-1}), (B) T (K), (C) normalized CH_4 concentration. (D)-(H): *YZ* slices (axes in m, at x = 0 m) through the reactor tube showing the gas T (K) fields around the foil with (D) an Ar only flow, flows with (E) 1%, (F) 10%, and, (G) 15% H_2 and, (H) a H_2 only flow. Arrows indicate foil location.

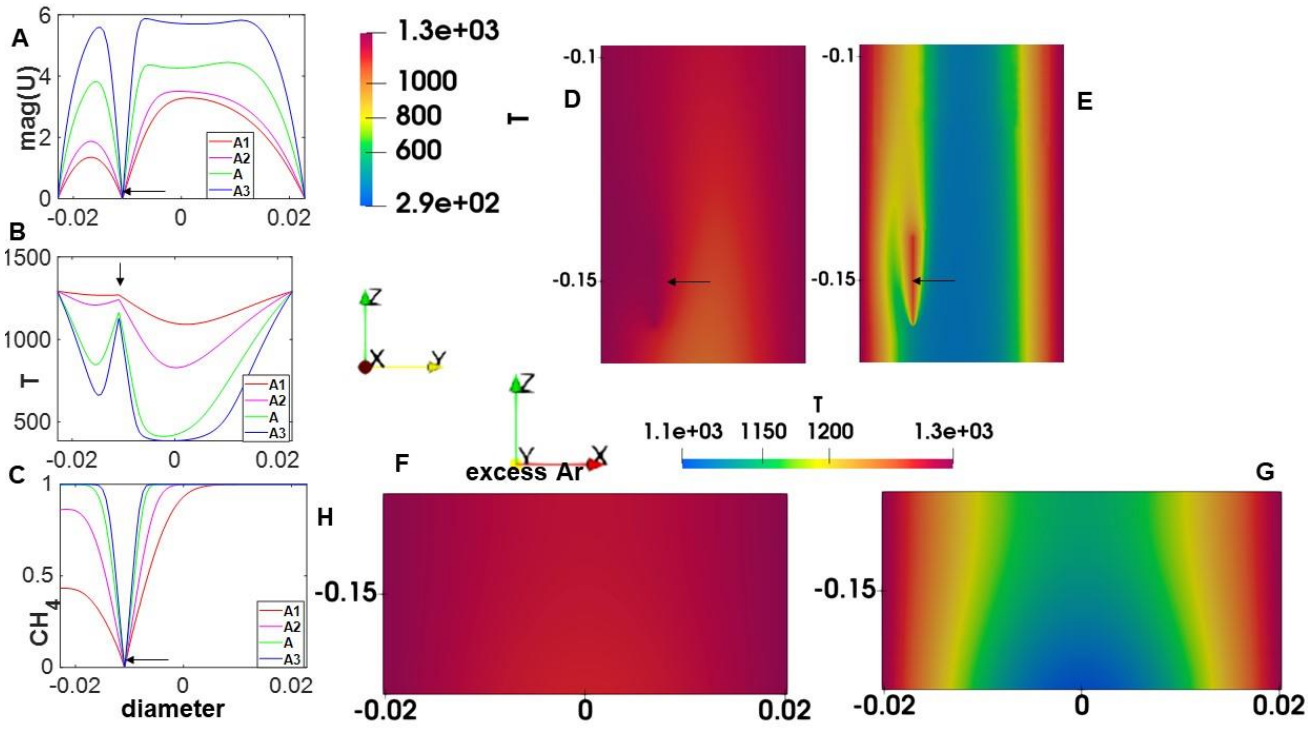

Figure 4. (A)-(C) Line profiles along the tube *y* diameter (m) at x = 0 m and across the center (at z = -0.15 m) of the 50 μm foil (with **foil setup A**) for different flow velocities and Ar proportions (both increase in order of A1, A2, A and A3): (A) mag(U) (ms^{-1}), (B) T (K), (C) normalized CH_4 concentration. (D)-(E): *YZ* slices (axes in m, at x = 0 m) through the reactor tube showing gas T (K) around the foil for: (F) A1, and, (G) A3. (G)-(H): Foil surface (axes in m) T (K) for (H) A1, and, (I) A3. Arrows indicate foil location.

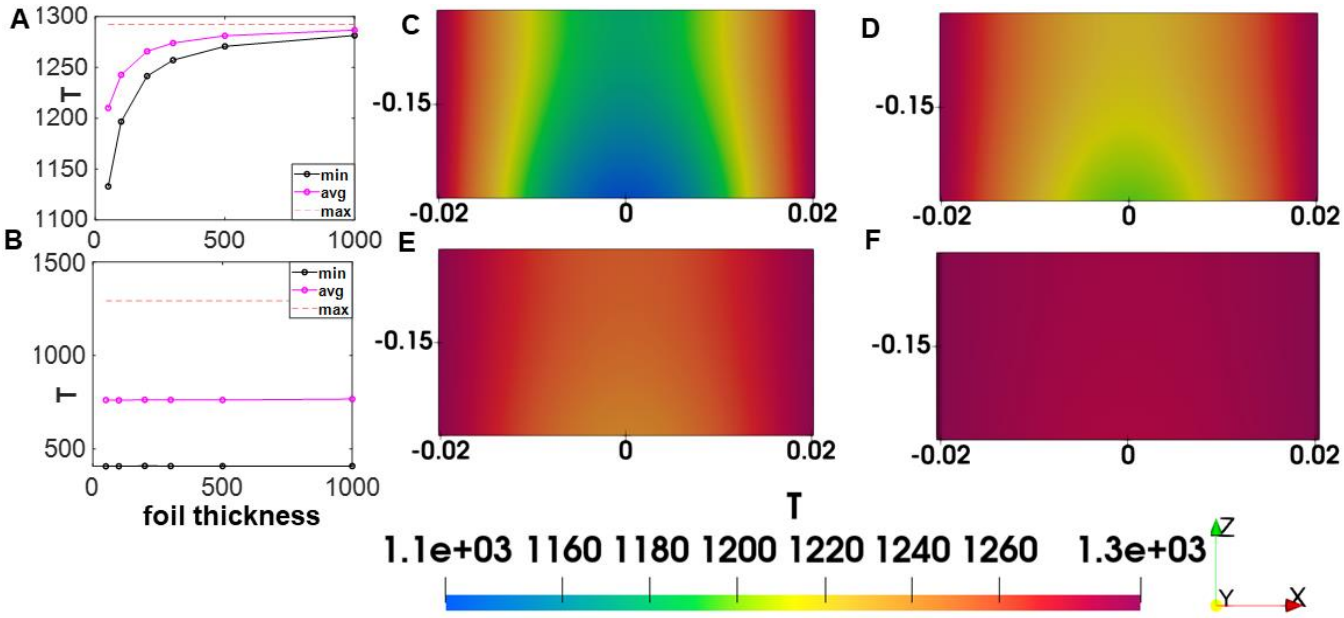

Figure 5. (A)-(B): Variation in *T* (K) with foil thickness for (A) foil, and (B) gas temperatures. (C)-(F) show the foil surface (axes in m) *T* (K) for 50 μm (C), 100 μm (D), 200 μm (E), and, 1 mm (F) thick foils.

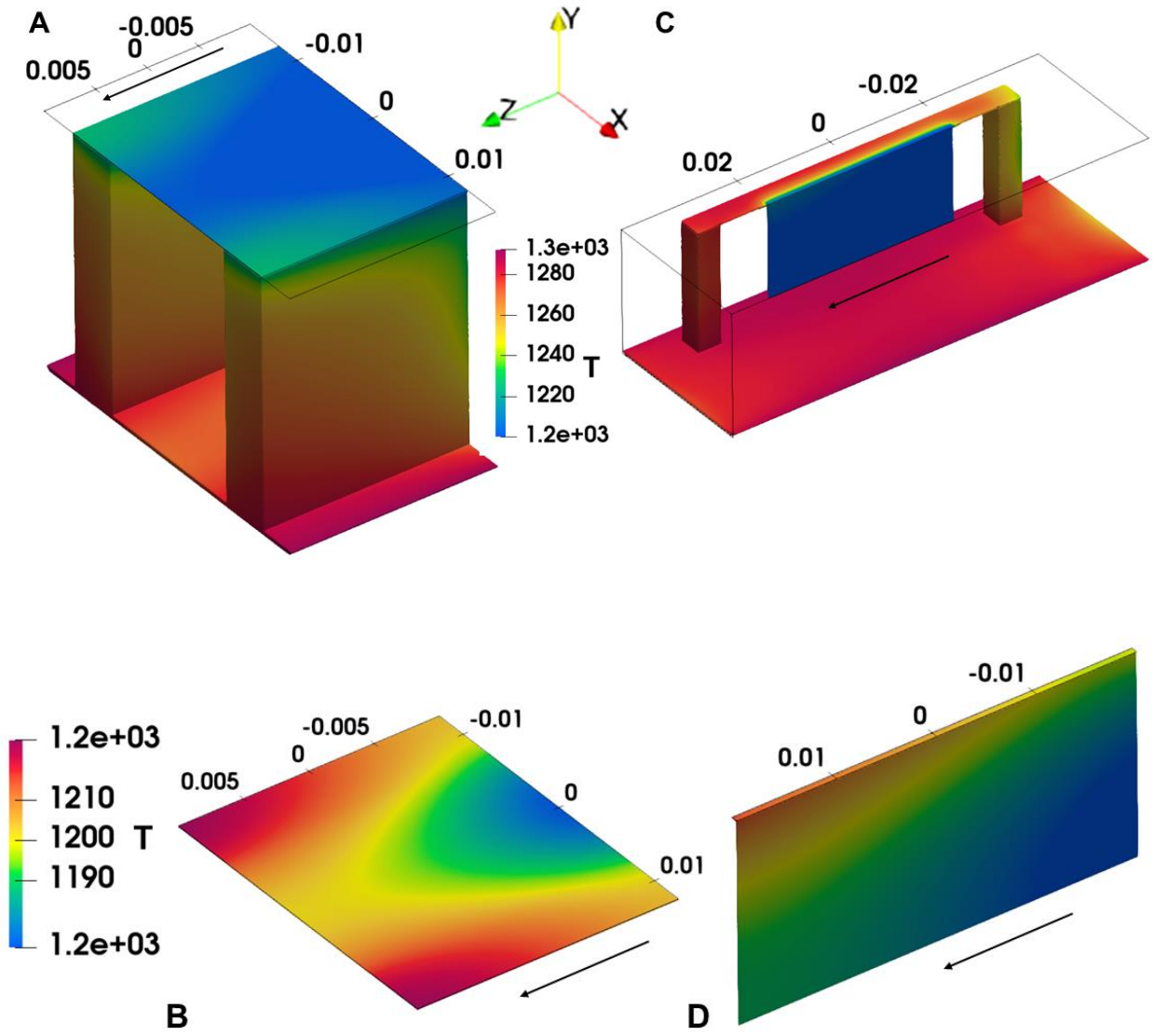

Figure 6. Temperature (K) distribution in 100 μm thick copper foils on quartz holders; (A)-(B) on a horizontal holder; (C)-(D) on a vertical holder. All axes are in m. Arrows indicate flow direction (*z* direction).

References

(1) Chatterjee, S.; Abadie, T.; Wang, M.; Matar, O. K.; Ruoff, R. S. Repeatability and Reproducibility in the Chemical Vapor Deposition of 2D Films: A Physics-Driven Exploration of the Reactor Black Box. *Chem. Mater.* **2024**, *36* (3), 1290–1298. DOI: 10.1021/acs.chemmater.3c02361.

(2) Greenshields, C.; Weller, H. *Notes on computational fluid dynamics*:*General principles*; CFD Direct Ltd, 2022.

(3) Moukalled, F.; Mangani, L.; Darwish, M. *The Finite Volume Method in Computational Fluid Dynamics*, Vol. 113; Springer International Publishing, 2016. DOI: 10.1007/978-3-319-16874-6.

(4) OpenFOAM. *OpenFOAM v2006*, 2020. https://www.openfoam.com/news/main-news/openfoam-v2006 (accessed 2020-06-30).

(5) Munson, B. R.; Young, D. F.; Okiishi, T. H. *Fundamentals of fluid mechanics*, 5th ed.; J. Wiley & Sons, 2006.